HHS Public Access

Author manuscript

Med Eng Phys. Author manuscript; available in PMC 2017 February 01.

Published in final edited form as:

Med Eng Phys. 2016 February ; 38(2): 72–79. doi:10.1016/j.medengphy.2015.11.004.

Automated pressure map segmentation for quantifying phalangeal kinetics during cylindrical gripping

Erik W. Sinsel[a,*], **Daniel S. Gloekler**[a,b], **Bryan M. Wimer**[a], **Christopher M. Warren**[a], **John Z. Wu**[a], and **Frank L. Buczek**[a,c]

[a]National Institute for Occupational Safety and Health (NIOSH), 1095 Willowdale Road MS 2027, Morgantown, WV 26505, USA

Abstract

Inverse dynamics models used to investigate musculoskeletal disorders associated with handle gripping require accurate phalangeal kinetics. Cylindrical handles wrapped with pressure film grids have been used in studies of gripping kinetics. We present a method fusing six degree-of-freedom hand kinematics and a kinematic calibration of a cylinder-wrapped pressure film. Phalanges are modeled as conic frusta and projected onto the pressure grid, automatically segmenting the pressure map into regions of interest (ROIs). To demonstrate the method, segmented pressure maps are presented from two subjects with substantially different hand length and body mass, gripping cylinders 50 and 70 mm in diameter. For each ROI, surface-normal force vectors were summed to create a reaction force vector and center of pressure location. Phalangeal force magnitudes for a data sample were similar to that reported in previous studies. To evaluate our method, a surrogate was designed for each handle such that when modeled as a phalanx it would generate a ROI around the cells under its supports; the classification F-score was above 0.95 for both handles. Both the human subject results and the surrogate evaluation suggest that the approach can be used to automatically segment the pressure map for quantifying phalangeal kinetics of the fingers during cylindrical gripping.

Keywords

Grip; Hand; Cylindrical handle; Pressure distribution; Pressure film

[*]Corresponding author. Tel.: +1 304 285 5834; fax: +1 304 285 6265. ESinsel@cdc.gov (E.W. Sinsel).
[b]Present address: University of Pittsburgh Medical Center (UPMC) Hamot, 201 State Street, Erie, PA 16550, USA
[c]Present address: Lake Erie College of Osteopathic Medicine (LECOM), 1858 West Grandview Blvd, Erie, PA 16509, USA

Conflict of interest statement
None of the authors of this paper have any conflict of interest.

Disclaimer
The findings and conclusions in this report are those of the authors and do not necessarily represent the views of the National Institute for Occupational Safety and Health.

Ethical approval
The study protocol was approved by the National Institute for Occupational Safety and Health (NIOSH) Human Subjects Review Board (HSRB) of the Centers for Disease Control and Prevention (CDC) Human Research Protection Office. Protocol identifier: HSRB 09-HELD-02XP.

1. Introduction

The forces and pressures experienced by the hand during tool use have been identified as important risk factors for hand related musculoskeletal disorders (MSDs) such as hand-arm vibration syndrome, carpal-tunnel syndrome, and hand/wrist tendinitis [1]. Understanding the relationships between these MSDs and hand forces during gripping requires accurate measurement of phalangeal kinetics [2–4]. More broadly, in studies of the kinetics of object manipulation, it is important to ensure accurate spatial registration of finger segments with instrumented contact surfaces [5–7].

Existing methods for measuring phalangeal kinetics generally involve either instrumenting the hand or instrumenting the contact surface. Instrumenting the hand includes such techniques as gloves with discrete sensors [8,9] or with sensor strips inserted into glove fingers [10], sets of pressure matrices [10] or a pressure mat attached to the hand [11], and distinct sensors attached to the hand [12]. Instrumenting the contact surface to acquire phalangeal kinetics includes using discrete sensors attached at specific locations [6,13–16], and covering the surface with a pressure sensitive mat or thin-film grid and applying either a manual [7,17–21] or automated feature-based [5] segmentation of the pressure distribution.

Gloves with a small number of individual sensors, and sensor matrices attached to the hand or a glove, have incomplete coverage of the contact area [10]; such methods often target data collection at the middle of each phalanx [8,9,12,14–16] which could alter the pressure distribution or not record pressures which have been observed to deviate from the middle of the phalanx [22,23]. The thickness of gloves can impact grip force output and distribution [24]; sensors of non-trivial thickness may alter the pressure distribution [11,12]. Techniques involving multiple sensors attached to the hand or glove may require cables or transmitters which can alter postures [10]. Devices instrumented with a small number of discrete sensors constrain finger placement, potentially altering the pressure distribution [6]. Techniques segmenting the pressure map into regions of interest (ROIs) through manual intervention introduce inter- and intra-segmenter variability in the creation of ROI boundaries [25–27]. Fully automated segmentation techniques based only on the pressure map create ROIs using inherent features of the pressure distribution; they do not provide spatial registration of finger phalanges and pressure cells, and thus cannot accurately locate ROI center of pressure (COP) relative to the contact anatomy.

Goislard de Monsabert et al. [19] wrapped a thin-film pressure grid around a 6-arm dynamometer handle and captured hand kinematics using retroreflective markers on the skin dorsal to finger joints. However, citing the complexity of fusing hand and pressure film kinematics, they used only thumb kinematics in calculating force vectors; the pressure map was manually segmented using inherent image features. Lee and Rim [22,23] combined cylindrical gripping kinematics and kinetics to assign pressure to phalanges. They used ink capsule film (Fuji Film, Fuji Photo Film USA Inc., New York) to collect peak pressure data, and applied black tape markers to the hand and markers to the cylinder to collect static kinematic data using synchronized photographic cameras. While similar, their approach has several important limitations. First, they used dorsal markers at joints to create and project finger segment lines which did not closely approximate the actual longitudinal bony

segments. Second, for each trial they manually aligned the film using markings on the handle. Third, they manually segmented the pressure distribution using a separate trial where the subject gripped a paper-covered handle with an inked hand, but provided no evaluation of either the film localization or segmentation. Finally, the film recorded only the maximum loading experienced by each ink capsule over the trial [23].

Inverse dynamics analyses used to study gripping related MSDs require quantification of the contact force between the hand and handle. In addition, the segmentation of the pressure map during gripping can further the understanding of the force distribution among the fingers, aiding ergonomic handle design. We present a method fusing hand and pressure film kinematics for the automated segmentation of a pressure map during gripping with minimal constraints on finger placement, allowing the quantification of phalangeal cylinder reaction forces, along with a center of pressure location, appropriate for use in inverse dynamics analyses.

2. Methods

2.1. Theoretical description

Thin-film pressure grids have been used previously in studies of gripping [2,5,18,19]. Our goal was to segment the pressure map into ROIs corresponding to overlying phalanges, principally of the index through little finger, based on rotational joint centers (Fig. 1A). We developed a fusion of hand kinematics supplied by motion capture markers, and kinetics supplied by a thin-film pressure grid wrapped around the handle and tracked with circular disk markers (Fig. 1B). First, we kinematically calibrated a pressure film coordinate system within the cylinder surface. Second, we utilized a six degree-of-freedom (6DOF) hand kinematic model in which frusta of cones are used to represent the phalanges [28] (Fig. 2A). In this model, segmental endpoints are created in a static calibration posture to approximate joint centers of rotation during dynamic trials. Frusta silhouettes were projected into the pressure grid to create ROIs which were used to calculate phalangeal integrated pressure, COP location, and cylinder reaction force (CRF) vectors. Finally, these data were combined with the hand kinematics in biomechanics software. A preliminary version of this work was presented at the American Society of Biomechanics annual meeting [29].

Two subjects (Table 1) were recruited within a research protocol approved by the agency Human Subjects Review Board, and provided informed consent. Kinematic data were collected at 100 Hz with a 14-camera Vicon MX-F40 optical motion capture system (Vicon Motion Systems Ltd., Oxford, England) with typical calibration accuracy better than 0.1 mm. Gripping kinetics were collected using two cylindrical aluminum handles with thin-film resistive pressure grids wrapped around them, 50 mm and 70 mm in diameter, created and calibrated using previously published methodology [2] (Fig. 1A). Each film contained a 44 × 44 grid of square cells 2.54 mm and 3.75 mm on a side, respectively (Tekscan, Inc., Boston MA, USA, models 5101 and 5150 N). Retroreflective hemispherical and circular disk markers were affixed to the handle and pressure film, respectively, for the creation of local coordinate systems. Pressure data were collected synchronously with the kinematics at 10 Hz.

The terminology used here is adapted from that of Pham et al. [27], used to describe the task of medical image segmentation.

Assigning pressure cells to ROIs which correspond to finger segments during gripping is similar to the task of classifying image pixels as having a particular property, such as being in the area of a tumor. In medical image analysis, the delineation of the pixel grid into regions is often based on inherent image features [27]. However, the task here was to generate anatomical ROIs from overlying finger segments, classifying pressure cell ROI membership independent of features of the pressure distribution.

Let Φ be the domain of pressure cells, each having a unique centroid location j in the pressure film coordinate system P, and let $\phi(j)$ be the recorded pressure value associated with location j. Our primary goal was to assign pressure cell locations to ROI sets R_k in Φ, where $k \in \{1, 2, \ldots, K\}$ corresponds to an anatomical ROI generated from one of K kinematically modeled phalanges, and $k = 0$ identifies the set of cells not assigned to an anatomical ROI. Pressure cells were assigned as members of one or more R_k based on the inclusion of the cell centroid within the ROI. For each R_k, a membership function, m_k, was created which defined the fractional amount of each cell's pressure value contained within the ROI.

The side length of the square pressure cells was more than an order of magnitude greater than the motion capture calibration residuals. To more closely match the pressure grid spatial resolution to motion capture system accuracy, each pressure cell was logically divided into a uniform $n \times n$ grid of subcells, with cell pressure uniformly distributed amongst all subcells. Spatial divisor $n = 10$ was found to provide a good balance between spatial resolution and computational complexity for single-thread execution on a personal computer (2.53 GHz Intel® Core i5 processor, 4GB memory). This logical division increased the accuracy of the partitioning of pressure cells by ROI boundaries, by the inclusion of subcells based on their centroid locations. In the case of a cell partially intersected by only one ROI boundary, the calculation of cell area within the ROI would have less than 5% error. Henceforth, the term *cell* will be used synonymously for any positive integer n.

2.1.1. Hand kinematics—A 6DOF hand kinematic model, developed by Buczek et al. [28], was implemented; 4 mm hemispherical markers were used to track the phalanges which were modeled as frusta of cones (Figs. 1B and 2A). In this model, to accommodate the visibility requirements of optical motion capture, joint calibration markers are located on dorsal and volar skin surfaces in the sagittal plane; inter-marker distance determines corresponding frusta diameters. Here, the frustum was used to provide a segment outline in a plane parallel to the handle axis during a power grip where coronal plane breadth is more relevant and has been shown to be consistently larger than sagittal plane depth at IP joints [31]. Therefore, in this study breadth measurements were used to determine frustum diameters; this modification did not affect the kinematic modeling. Frusta diameters were determined using a 12 megapixel digital photograph of the hand flat on a table with the palm down and fingers extended; the camera's optical axis was perpendicular to the table with anthropometric scales in view. Diameters at IP joints were determined using finger width at the dorsal joint calibration marker. The diameter at the fingertip was determined using tangent lines drawn distally from the distal IP (DIP) joint and intersecting a transverse line

drawn tangent to the fingertip. At metacarpophalangeal (MCP) joints, the midpoints between the MCP markers of adjacent fingers was marked and the distance between adjacent midpoints was used as the diameter, except for the index and little fingers where the lateral and medial aspect markers, respectively, were used instead of a midpoint mark. This manual volumetric calibration of the model is similar to the manual application of joint calibration markers used to locate segment endpoints during gripping trials; it does not affect the automated nature of the creation of ROIs in the pressure map.

2.1.2. Pressure film kinematics—For each matching motion capture and pressure film sample, several local reference frames were created (Fig. 2B). Calibration disk marker coordinates in reference frame S and their corresponding nominal row and column pressure cell coordinates were used to calibrate the 2-D pressure film coordinate system, P(*r*, *c*), where *r* and *c* were Real-valued; e.g., the cell in the first row and column had centroid location $j_{1,1}$ = (0.5, 0.5).

A linear least-squares optimization was performed to calculate the orientation angle (α) and create a row-format orthonormal orientation matrix of P in S:

$$ {}^{\mathrm{S}}\mathbf{R}_{\mathrm{P}} = \begin{bmatrix} \cos(\alpha) & -\sin(\alpha) \\ \sin(\alpha) & \cos(\alpha) \end{bmatrix}. \quad (1) $$

Pressure cell side length *d* and cell spatial divisor *n* were used to create a scaling matrix:

$$ {}^{\mathrm{S}}\mathbf{D}_{\mathrm{P}} = \begin{bmatrix} n/d & 0 \\ 0 & n/d \end{bmatrix} \quad (2) $$

Establishing the translation between coordinate systems requires a point whose coordinates are known in both systems. This is often the origin of one system, although any common point may be used. To reduce errors associated with marker-based tracking, when the coordinates of multiple points are known in both systems it is preferable to use their centroid instead of a single point [33]. The correspondence between the disk markers' centroid in S, ${}^{\mathrm{S}}\bar{\mathbf{m}}$, and their nominal cell centroid, ${}^{\mathrm{P}}\bar{\mathbf{m}}$, was used to locate the origin of P in S:

$$ {}^{\mathrm{s}}\mathbf{l} = {}^{\mathrm{S}}\bar{\mathbf{m}} - {}^{\mathrm{P}}\bar{\mathbf{m}}\left[{}^{\mathrm{S}}\mathbf{R}_{\mathrm{P}}\right]^{-1}\left[{}^{\mathrm{S}}\mathbf{D}_{\mathrm{P}}\right]^{-1}. \quad (3) $$

Using Eqs. (1)–(3), a row-format surface position vector, ${}^{\mathrm{S}}\mathbf{r}_j$, could be transformed into a Real-valued pressure cell position vector:

$$ {}^{\mathrm{P}}\mathbf{r}_j = \left({}^{\mathrm{S}}\mathbf{r}_j - {}^{\mathrm{S}}\mathbf{l}\right) {}^{\mathrm{S}}\mathbf{R}_{\mathrm{P}}\, {}^{\mathrm{S}}\mathbf{D}_{\mathrm{P}}. \quad (4) $$

The precision of the pressure film kinematic calibration was assessed by calculating the root-mean-square error (RMSE) of calibration markers with nominal cell centroids. The pressure film had been permanently adhered to the handle in a prior study, complicating the

assessment of calibration marker accuracy. The calibration process was replicated three times using a setup similar to that of the 50 mm handle, using a lightly-taped pressure film which was removed after each calibration to measure marker placement accuracy.

2.1.3. Silhouette projection and ROI creation—A trapezoidal silhouette of the phalanx frustum was created by the intersection of its long axis with a plane parallel to the cylindrical axis (Fig. 2B). Silhouette vertices were projected onto the surface orthogonally to the cylindrical axis and the surface. Using Eq. (4), projected vertex points in S were transformed into Real-valued row and column coordinates in P, and were linearly interpolated to create a ROI. At IP joints, the ROIs were typically not perfectly mated. This was expected due to the use of a 6DOF hand model and to the orientations of the flexed fingers relative to the cylindrical axis. In order to more realistically represent the contact anatomy, ROIs at IP joints were connected by a shared boundary using the midpoints of respective adjacent medial and lateral vertices.

2.1.4. Region of interest set membership—For each anatomical ROI, R_k, where $k \in \{1, 2, \ldots, K\}$, and for all centroid locations j, there was an initial pressure cell set membership function:

$$m_k^{\circ}(j) = \begin{cases} 1, & if\ j \in R_k \\ 0, & otherwise. \end{cases} \quad (5)$$

Additionally, all cells which were not members of an anatomical ROI were contained in a non-anatomical ROI, R_0, with an initial membership function:

$$m_0^{\circ}(j) = \begin{cases} 0, & if\ j \in \bigcup_{k=1}^{K} R_k \\ 1, & otherwise. \end{cases} \quad (6)$$

Initially all membership functions had binary range {0, 1}. If there were no overlapping ROIs, the membership functions m_k° would preserve the unity of pressure in Φ. However, overlapping regions were allowed and expected. Therefore, we apportioned the cell pressure value equally among overlapping regions, resulting in final membership functions for all j, k:

$$m_k(j) = \frac{m_k^{\circ}(j)}{\sum_{k=0}^{K} m_k^{\circ}(j)}. \quad (7)$$

The combination of Eqs. (5) and (6) ensured that $\forall j, \exists k, m_k^{\circ}(j) = 1$, or that every cell was contained within at least one ROI. Therefore, Eq. (7) ensured that $\forall j, \forall k, 0 \le m_k(j) \le 1$, and $\forall j, \sum_{k=0}^{K} m_k(j) = 1$, or that the unity of pressure was preserved while allowing overlapping anatomical ROIs.

An outward-pointing unit vector normal to the cylinder surface, ${}^{\mathrm{C}}\mathbf{n}_j$, was created at each cell centroid, and the resultant cylinder reaction force vector was calculated for each R_k:

$$ {}^{\mathrm{C}}\mathbf{f}_k = \sum_{j \in R_k} m_k(j)\, \varphi(j)\, A\, {}^{\mathrm{C}}\mathbf{n}_j, \quad (8) $$

where A was the cell area. The force vector was transformed into laboratory coordinates. The COP was calculated using cell centroid position vectors:

$$ {}^{\mathrm{P}}\mathbf{c}_k = \frac{\sum_{j \in R_k} \varphi(j)\, {}^{\mathrm{P}}\mathbf{r}_j}{\sum_{j \in R_k} \varphi(j)}. \quad (9) $$

Using the inverse of Eq. (4), the COP was transformed into S and ultimately into laboratory coordinates.

2.1.5. Phalanx surrogate validation—Direct validation of image segmentation tasks is often confounded by the lack of a feasible gold standard method providing a ground truth segmentation [25,34]. Surrogates for human anatomy have been used to provide experimental control in evaluating image segmentation algorithms and imaging systems [25,27,35–37]. We constructed a phalanx surrogate for each handle (Fig. 3A). The surrogate exerted pressure through two supports, each of which was slightly less than a column in width and a multiple of rows in height. Tracking and calibration markers were attached to replicate the modeling of a phalanx, kinematic calibration data were collected, and calibration markers removed. The surrogate was attached to the handle and kinematic and pressure data were collected (Fig. 3B). Thin strips of a high-friction cushioning material were incorporated between the supports and pressure film and were included in the design.

The surrogate was attached such that each support lay within a single column and along a number of rows which defined the actual ROI, R_A. The surrogate was designed to produce a projected ROI encompassing the cells under and between its supports, defining the hypothesized ROI, R_H. Using the same method as with human subject data, a hypothesized ROI was generated for surrogate trials (Fig. 3C). The goal in the surrogate trial was to perform a binary classification of pressure cells as being either inside or outside of R_A. This task can be seen as hypothesizing the case's membership in one of two ground truth sets, "positive" or "negative" (P or N) for a cell centroid being respectively inside or outside of R_A. By comparison with the ground truth, the classification of each cell was evaluated to be true or false, leading to four possible outcome sets, defined in Fig. 4.

Binary classification outcomes are closely related to statistical hypothesis testing [38]. The frequency of correctly classified positive cases is called the true positive rate: $TPR = |TP|/|P|$, where vertical bars denote set cardinality or number of members. TPR is also known as *sensitivity*, the statistical power and complement of the probability of a "Type II" error. The frequency of correctly classified negative cases is called the true negative rate: $TNR = |TN|/|N|$. TNR is also known as *specificity*, the complement of the probability of a "Type I" error. Sensitivity and specificity are often used together to characterize a classifier's tradeoff between true positives and false positives. In our case the number of negative cells, $|N|$, is

influenced by the size of the pressure film grid and so *TNR* would arbitrarily depend on the pressure film model. However, since the ideal of *TPR* = 1 can be achieved by setting $R_H = \Phi$, using *TPR* alone is insufficient. An additional performance measure is *precision*, which is the proportion of true positives in R_H: *precision* = |*TP*|/(|*TP*| + |*FP*|). The unweighted first harmonic mean of *TPR* and *precision*, known as the F-measure or F-score [38], has been used to describe classification performance independent of |*N*|:

$$F_1 = \frac{2}{1/precision + 1/TPR}. \quad (10)$$

Substituting the set theoretic formulations in Fig. 4,

$$TPR = \frac{|R_A \cap R_H|}{|R_A|}, \quad (11)$$

and

$$precision = \frac{|R_A \cap R_H|}{|R_H|}. \quad (12)$$

Substituting Eqs. (11) and (12) into Eq. (10) and simplifying, we express F_1 in terms of ROI sets:

$$F_1 = \frac{2|R_A \cap R_H|}{|R_A| + |R_H|}. \quad (13)$$

The numerator of Eq. (13) rewards achieving true positives, while the denominator penalizes doing so by creating an overly large R_H. The range of F_1 is [0, 1], where the ideal result of $F_1 = 1$ is obtained if and only if $R_H = R_A$. Using Eq. (13), F_1 was calculated for a single trial using each handle and the surrogate designed for it.

2.2. Experimental protocol

After the subject provided informed consent, anthropometric measurements were taken of the right hand, and motion capture markers were applied. Dorsal photographs were taken of the hand resting flat on a tabletop with the fingers extended, a pose similar to the subsequent kinematic calibration. Markers used only for calibration were removed and the subject performed a maximum power grip with their dominant right hand for 10 seconds on each handle (Fig. 1A). The trial length was to allow subjects time to achieve a quasi-static exertion level based on total grip force. Subjects were instructed to grip such that the thumb did not overlap, and exert pressure on, other digits. Experimenters verified the hand position on the pressure film to ensure data collection under the fingers, as has been done in other studies of gripping [2,7,20,22]. Neither the hand-arm system nor the handle were fixed in space; excellent visibility of the motion capture markers was observed, with the vast majority being tracked by at least three cameras. The “6DHand” 6DOF kinematic model and

marker set developed by Buczek et al. [28] was used for the hand kinematics (Fig. 1B). Kinematic modeling was performed in Visual3D; kinematics and pressure data were imported into MATLAB (The MathWorks, Inc., Natick MA, USA, version 2009a) for analysis.

3. Results

Pressure maps with anatomical ROIs are presented for four trials involving two subjects and two handle sizes (Fig. 5). The subjects differed greatly in both body mass and hand length (Table 1). Human trial results show strong qualitative correspondence between pressure film ROIs and overlying anatomy, with the ROIs containing nearly all suprathreshold pressure within recognizable anatomical patterns. ROI boundary locations also demonstrate the transparency of the method to inherent features of the pressure map; some IP joint boundaries cross through areas of no measured pressure, while others cross through areas of relatively homogenous local pressure. Force magnitudes are presented (Fig. 6A) for the sample pressure data shown in Fig. 5C. The force vectors were applied to the hand at the corresponding COP locations, in modeling software (Fig. 6B).

Pressure film kinematic calibration RMSE are presented for the four trials shown in Fig. 5 and for the replicated calibrations (Table 2). Mean RMSE values were less than 0.5 mm, with standard deviations less than 0.02 mm. The calibration replication study produced similar precision, with mean RMSE less than 0.5 mm, and mean error vector magnitude and standard deviation were less than 0.2 mm for all three replications. The maximum error vector magnitude across all replicated calibrations was less than 10% of the length of a cell side. Standard deviations were higher along the row axis, which was aligned with the cylindrical axis, where marker placement relied on more obscure visible landmarks than along the column axis.

The hypothesized ROIs of the surrogate trials closely matched the actual ROIs, with $F_1 > 0.95$ for both handles (Table 3). The largest sources of error were likely in the surrogate fabrication and its attachment. Notwithstanding these potential sources of error, similarly high performance was demonstrated for both handles which were of different diameters and wrapped with different pressure film models.

4. Discussion and conclusions

In the current study, we proposed a method to extract the contact forces applied on the finger segments in gripping test, wherein a pressure grid on the handle was kinematically calibrated for the fusion of hand kinematics and kinetics resulting in the automated creation of phalangeal regions of interest in the pressure film. The calculated contact force on the segments of the index through little finger for a male subject maximally gripping a 50 mm handle (Fig. 6A) are consistent with the mean contact force reported in previous studies [15,16,19,23]. However, differences in results may be expected due to methodological differences. In particular, Amis [15] collected force data from independent trials, one per finger, not all fingers simultaneously. Radhakrishnan and Nagaravindra [16] used four parallel arcs of discrete sensor pads, with a pad near the middle of each phalanx, which constrained the grip posture and potentially altered the force distribution. Our technique

does not constrain the grip posture to accommodate discrete sensors and the use of a pressure film provides more complete coverage of the finger contact area. Total finger force is consistent with that reported by Goislard de Monsabert et al. [19], who used a similar pressure film with a manual segmentation method; however a detailed comparison of the forces applied on the finger segments is not possible, as different anatomical bases were used for segmenting the pressure distribution.

Phalangeal normal force is also generally consistent with that reported by Lee and Rim [22,23], whose method was mathematically similar to that presented here. However, they used ink capsule film, which records the maximum loading on each capsule during the trial. Additionally, they used skin markers dorsal to finger joints to create segment lines. Projections of dorsal segment lines can cause errors, particularly in COP locations, when the plane of flexion is not aligned with the cylinder transverse plane – an orientation illustrated by the index finger of subject A in our study (see Fig. 5A and B). Our method uses a 6DOF hand model to provide segment lines which approximate the bony segment. In addition, their method involved a manual segmentation of the pressure map which is not explained in detail or evaluated. Rossi et al. [20] combined a handle with integrated sensors for measuring total grip force with an overlying pressure mat to provide a total grip force-normalized pressure distribution, however they used a manual segmentation technique based on subject anthropometry. Our approach can improve the localization and segmentation of pressure data in such sensor fusion. Automated image segmentation techniques based on inherent image features fail in regions of homogenous data, such as in areas of sub-threshold pressure (see Fig. 5A, little finger distal IP joint), and in areas where the ROI boundary crosses a contiguous region of pressure (see Fig. 5C, thumb IP joint). By combining hand and pressure film kinematics, our technique is capable of creating ROIs independent of the inherent features of the pressure distribution.

The segmentation performance relies principally on the accuracy of the human kinematic modeling, the accuracy of the pressure film kinematic calibration, and on the projection of frusta silhouettes. The kinematic performance of the 6DHand model, including the trials used here, has been described elsewhere for the index through little finger [28]. For 20 subjects lightly gripping a handle 30 mm in diameter, the reported means and standard deviations of translations at IP joints were less than 2 mm. The accuracy of the pressure film kinematic calibration could not be directly measured as the film had been permanently adhered to the handles. However, the replicated calibrations, performed by the same experimenter who kinematically calibrated the handles used for subject trials, demonstrated consistently high accuracy, and RMSE values were similar to those observed in subject trials (Table 2). Our method involved modeling phalanges as frusta whose silhouettes were mathematically projected onto the pressure film. The resulting ROI could encompass cells which do not lie under the contact anatomy, and ROIs of adjacent digits could overlap. In other studies involving the segmentation of pressure maps generated by the hands or feet, it is common for segmentation regions to encompass area not in direct contact with overlying anatomy [18–21]. An individuated surface model, such as via 3-D finger scan, could provide more accurate projections. However, such geometric errors would be primarily in the longitudinal ROI borders where observed pressure values were relatively low (see Fig. 5). Also, total contact area changes with total grip force output and handle diameter [39,40]. It

seems likely that any method wherein a static geometric model is projected onto the pressure map during a dynamic trial would result in ROIs which do not precisely fit the contact area. Further, the inclusion of cells of subthreshold pressure in an ROI would have no change on the force and COP calculations in Eqs. (8) and (9), as these are not directly affected by ROI area.

The pressure films did not completely cover the handles; that limitation was a byproduct of the combination of handle and pressure film and was not inherent to the approach. Also, since inverse dynamics analysis is mainly intended to investigate the musculoskeletal loading in the fingers and thumb, which is relevant to the MSDs, the contact forces at the palm are not important. It is well accepted that the musculoskeletal loading in the fingers is minimized for a handle diameter of approximately 40 mm [39,41]. A smaller handle size (e.g., <30 mm) is rarely used in tool design because of ergonomic reasons. Therefore, we have not considered the effects of the finger overlap when gripping on such small handles. The pressure film models lacked shear force information, although shear may cause local variations in the grip force distribution, especially with high-friction handle surfaces. Enders and Seo [14] observed a 22% mean increase in proximal-distal shear force and a 4% mean increase in phalanx normal force when subjects gripped a cylindrical handle 51 mm in diameter covered in rubber as opposed to paper (for both 50% and maximum exertion). Notwithstanding these limitations, reasonable accuracy was demonstrated in both qualitative and quantitative evaluations, suggesting that this approach provides a good first approximation of phalangeal kinetics during gripping on a cylindrical handle.

Acknowledgments

Funding

This work was funded by the National Institute for Occupational Safety and Health (NIOSH), U.S.A.

The authors thank Elizabeth Kyonka for her helpful discussion of an earlier version of the manuscript.

Nomenclature

Φ	domain of pressure cell centroids j
d	pressure cell side length
n	pressure cell spatial divisor
C, S, P	local reference frames for cylinder, cylinder surface, and pressure film
x, y, z, s, r, c	coordinate system axes
${}^{S}\mathbf{r}_j$, ${}^{P}\mathbf{r}_j$, ${}^{S}\mathbf{l}$	row-format position vectors with reference frame superscript
${}^{S}\mathbf{m}, {}^{P}\mathbf{m}$	pressure cell calibration marker centroid position vectors
α	orientation angle of P in S
${}^{S}\mathbf{R}_P$	orthonormal orientation matrix of P in S
${}^{S}\mathbf{D}_P$	scaling matrix from S to P

$\phi(j)$	pressure value for cell at location j
R_k	ROI set k in Φ
m_k	membership function for R_k
$\lvert R_k \rvert$	set cardinality
$\lVert \mathbf{e} \rVert$	vector magnitude
$\forall, \exists.$	quantifiers: universal, existential
$\cup, \cap, \in$	set operators: union, intersection, membership
TP, FP, TN, FN	classification outcome sets
TPR, TNR	true positive rate, true negative rate
F_1	unweighted F-score
p_k	integrated pressure for R_k
${}^{C}\mathbf{f}_k$	cylinder reaction force vector for R_k
${}^{P}\mathbf{c}_k$	center of pressure position vector for R_k

References

1. NIOSH. Musculoskeletal disorders and workplace factors: a critical review of epidemiologic evidence for work-related musculoskeletal disorders of the neck, upper extremity, and low back. Cincinnati, OH: U.S. Department of Health and Human Services, National Institute for Occupational Safety and Health; 1997. NIOSH Publication 97-141
2. Dong RG, Wu JZ, Welcome DE, McDowell TW. A new approach to characterize grip force applied to a cylindrical handle. Med Eng Phys. 2008; 30:20–33. [PubMed: 17339124]
3. Wu JZ, Dong RG, McDowell TW, Welcome DE. Modeling the finger joint moments in a hand at the maximal isometric grip: the effects of friction. Med Eng Phys. 2009; 31:1214–18. [PubMed: 19700363]
4. Wu JZ, Sinsel EW, Gloekler DS, Wimer BM, Zhao KD, An KN, et al. Inverse dynamic analysis of the biomechanics of the thumb while pipetting: a case study. Med Eng Phys. 2012; 34:693–701. [PubMed: 22015316]
5. Kutz DF, Wölfel A, Timmann D, Kolb FP. Detection of changes in grip forces on a sliding object. J Neurosci Methods. 2007; 166:250–8. [PubMed: 17765320]
6. Zhang W, Gordon AM, McIsaac TL, Santello M. Within-trial modulation of multi-digit forces to friction. Exp Brain Res. 2011; 211:17–26. [PubMed: 21455619]
7. Pataky TC, Slota GP, Latash ML, Zatsiorsky VM. Radial force distribution changes associated with tangential force production in cylindrical grasping, and the importance of anatomical registration. J Biomech. 2012; 45:218–24. [PubMed: 22134182]
8. Gulke J, Wachter NJ, Katzmaier P, Ebinger T, Mentzel M. Detecting submaximal effort in power grip by observation of the strength distribution pattern. J Hand Surg Eur. 2007; 32:677–83.
9. Kong Y-K, Lowe BD. Optimal cylindrical handle diameter for grip force tasks. Int J Ind Ergon. 2005; 35:495–507.
10. Lemerle P, Klinger A, Cristalli A, Geuder M. Application of pressure mapping techniques to measure push and gripping forces with precision. Ergonomics. 2008; 51:168–91. [PubMed: 17896224]
11. Dale AM, Rohn AE, Patton A, Standeven J, Evanoff B. Variability and misclassification of worker estimated hand force. Appl Ergon. 2011; 42:846–51. [PubMed: 21349496]

12. Pylatiuk C, Kargov A, Schulz S, Doderlein L. Distribution of grip force in three different functional prehension patterns. J Med Eng Technol. 2006; 30:176–82. [PubMed: 16772221]
13. Ambike SS, Paclet F, Latash ML, Zatsiorsky VM. Grip-force modulation in multi-finger prehension during wrist flexion and extension. Exp Brain Res. 2013; 227:509–22. [PubMed: 23625077]
14. Enders LR, Seo NJ. Phalanx force magnitude and trajectory deviation increased during power grip with an increased coefficient of friction at the hand-object interface. J Biomech. 2011; 44:1447–53. [PubMed: 21496820]
15. Amis AA. Variation of finger forces in maximal isometric grasp tests on a range of cylinder diameters. J Biomed Eng. 1987; 9:313–20. [PubMed: 3682795]
16. Radhakrishnan S, Nagaravindra M. Analysis of hand forces in health and disease during maximum isometric grasping of cylinders. Med Biol Eng Comput. 1993; 31:372–6. [PubMed: 8231299]
17. Aldien Y, Welcome D, Rakheja S, Dong R, Boileau PE. Contact pressure distribution at hand–handle interface: role of hand forces and handle size. Int J Ind Ergon. 2005; 35:267–86.
18. Nicholas JW, Corvese RJ, Woolley C, Armstrong TJ. Quantification of hand grasp force using a pressure mapping system. Work. 2012; 41(Suppl 1):605–12. [PubMed: 22316789]
19. Goislard de Monsabert B, Rossi J, Berton E, Vigouroux L. Quantification of hand and forearm muscle forces during a maximal power grip task. Med Sci Sports Exerc. 2012; 44:1906–16. [PubMed: 22617399]
20. Rossi J, Berton E, Grelot L, Barla C, Vigouroux L. Characterisation of forces exerted by the entire hand during the power grip: effect of the handle diameter. Ergonomics. 2012; 55:682–92. [PubMed: 22458871]
21. Seo NJ, Armstrong TJ, Ashton-Miller JA, Chaffin DB. The effect of torque direction and cylindrical handle diameter on the coupling between the hand and a cylindrical handle. J Biomech. 2007; 40:3236–43. [PubMed: 17570375]
22. Lee JW, Rim K. A new method for measurement of finger-phalangeal force. Exp Mech. 1990; 30:392–7.
23. Lee JW, Rim K. Measurement of finger joint angles and maximum finger forces during cylinder grip activity. J Biomed Eng. 1991; 13:152–62. [PubMed: 2033951]
24. Wimer B, McDowell TW, Xu XS, Welcome DE, Warren C, Dong RG. Effects of gloves on the total grip strength applied to cylindrical handles. Int J Ind Ergon. 2010; 40:574–83.
25. Maintz JB, Viergever MA. A survey of medical image registration. Med Image Anal. 1998; 2:1–36. [PubMed: 10638851]
26. Markelj P, Tomazevic D, Likar B, Pernus F. A review of 3D/2D registration methods for image-guided interventions. Med Image Anal. 2012; 16:642–61. [PubMed: 20452269]
27. Pham DL, Xu C, Prince JL. Current methods in medical image segmentation. Annu Rev Biomed Eng. 2000; 2:315–37. [PubMed: 11701515]
28. Buczek FL, Sinsel EW, Gloekler DS, Wimer BM, Warren CM, Wu JZ. Kinematic performance of a six degree-of-freedom hand model (6DHand) for use in occupational biomechanics. J Biomech. 2011; 44:1805–9. [PubMed: 21530970]
29. Sinsel, EW.; Gloekler, DS.; Wimer, BM.; Warren, CM.; Wu, JZ.; Buczek, FL. A novel technique quantifying phalangeal interface pressures at the hand-handle interface. Proceedings of the American Society of Biomechanics 34th annual meeting; Providence, RI. August 2010;
30. Buchholz B, Armstrong TJ, Goldstein SA. Anthropometric data for describing the kinematics of the human hand. Ergonomics. 1992; 35:261–73. [PubMed: 1572336]
31. Buchholz B, Armstrong TJ. An ellipsoidal representation of human hand anthropometry. Hum Factors. 1991; 33:429–41. [PubMed: 1955203]
32. Salomon, D. Transformations and projections in computer graphics. London: Springer; 2006.
33. Horn BKP, Hilden HM, Negahdaripour S. Closed-form solution of absolute orientation using orthonormal matrices. J Opt Soc Am. 1988; 5:1127–35.
34. Udupa JK, LeBlanc VR, Ying ZG, Imielinska C, Schmidt H, Currie LM, et al. A framework for evaluating image segmentation algorithms. Comput Med Imag Grap. 2006; 30:75–87.

35. Bernstein KR, Matthews KL, Morrow AN, Smith BM, Bujenovic LS. ROC analysis of PET imaging performance of two PET/CT scanners based on lesion detectability in a torso phantom. IEEE Nucl Sci Conf R. 2006:2636–43.

36. Boellaard R, Krak NC, Hoekstra OS, Lammertsma AA. Effects of noise, image resolution, and ROI definition on the accuracy of standard uptake values: a simulation study. J Nucl Med. 2004; 45:1519–27. [PubMed: 15347719]

37. Shcherbinin S, Celler A. An enhancement of quantitative accuracy of the SPECT/CT activity distribution reconstructions: physical phantom experiments. Comput Med Imaging Graph. 2010; 34:346–53. [PubMed: 20060683]

38. Fawcett T. An introduction to ROC analysis. Pattern Recogn Lett. 2006; 27:861–74.

39. Seo NJ, Armstrong TJ. Investigation of grip force, normal force, contact area, hand size, and handle size for cylindrical handles. Hum Factors. 2008; 50:734–44. [PubMed: 19110833]

40. Welcome D, Rakheja S, Dong R, Wu JZ, Schopper AW. An investigation on the relationship between grip, push and contact forces applied to a tool handle. Int J Ind Ergon. 2004; 34:507–18.

41. Edgren CS, Radwin RG, Irwin CB. Grip force vectors for varying handle diameters and hand sizes. Hum Factors. 2004; 46:244–51. [PubMed: 15359674]

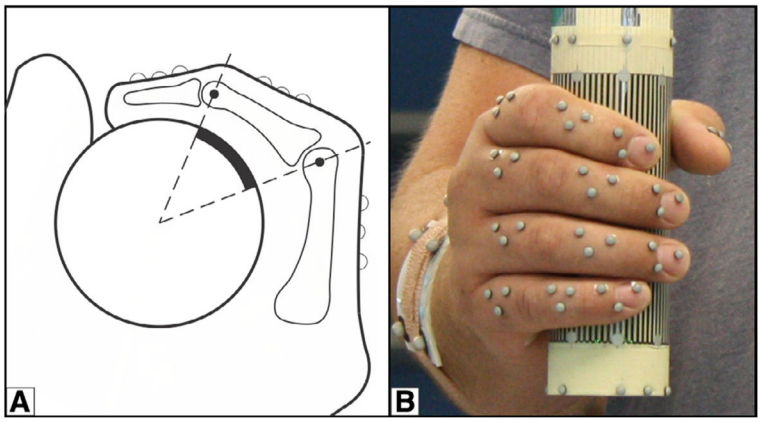

Fig. 1.

Experimental setup. (A) Cross-sectional illustration of a finger during gripping, with the distal, middle, and proximal phalanges. (B) A subject gripping the 50 mm handle. The segmental contact area is defined using estimates of the joint centers of rotation (CORs). Hemispherical (4 mm) markers were used to kinematically calibrate segment endpoints at CORs, and track the finger segments and cylinder. Circular disk (5 mm) markers were used to calibrate the pressure film coordinate system.

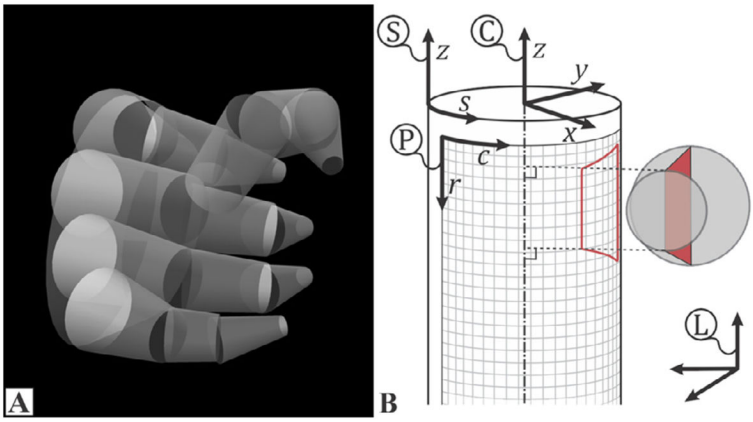

Fig. 2.

Kinematic analysis. (A) Kinematic modeling of the trial in Fig. 1B, in Visual3D software (C-Motion Inc., Germantown MD, USA), using the 6DOF hand kinematic model "6DHand" [28]. (B) Coordinate systems and frustum silhouette projection onto the pressure film. Hemispherical markers on the cylinder were used to calibrate the cylinder 3-D coordinate system, C(*x,y,z*), in the laboratory (L), where the *z*-axis was aligned with the cylinder longitudinal axis. The surface of a cylinder may be conceptually unrolled and mathematically treated as a 2-D plane [32]. The 2-D cylinder surface coordinate system, S(*s,z*) was created through a parameterization of C. The pressure film was assumed to be coincident with the cylinder surface and was treated as a 2-D grid in S. Disk marker coordinates in S were used to calibrate the pressure film row and column coordinate system P(*r,c*). The frustum silhouette was projected orthogonally onto S and transformed into P to create an anatomical ROI in the pressure film.

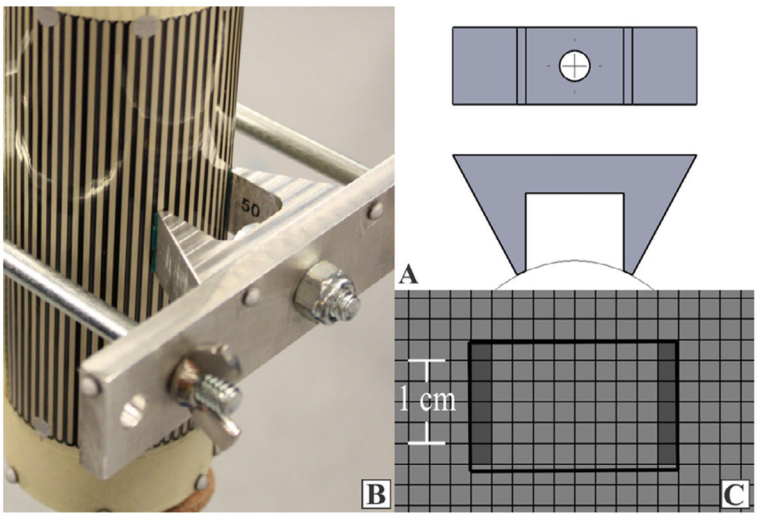

Fig. 3.

Phalanx surrogate design (A), trial setup (B), and graphical result (C) for the 50 mm handle. The pressure map is presented in binary scaling for clarity, with the actual ROI defined by activated cells and the hypothesized ROI boundary drawn with a solid black line. The same algorithm was applied as with the human subject data. Square pressure cell sides were 2.54 mm.

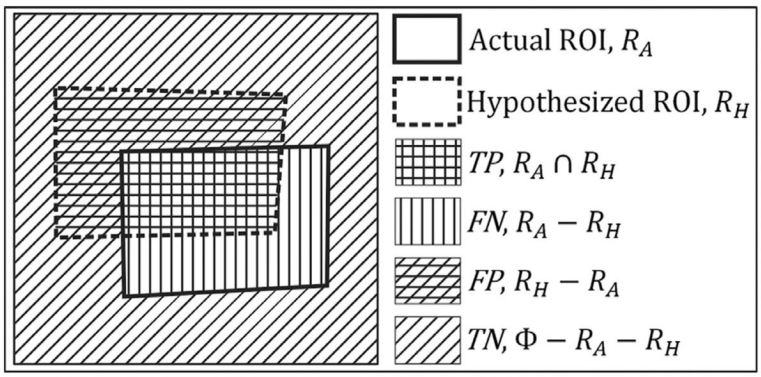

Fig. 4.

Binary classification outcomes in set theoretic formulations. True positive (*TP*), false positive (*FP*), true negative (*TN*), and false negative (*FN*) outcome sets are defined by the intersection of ROI sets R_H and R_A within pressure cell domain Φ. An individual pressure cell is included as a member of the appropriate set based on its centroid location.

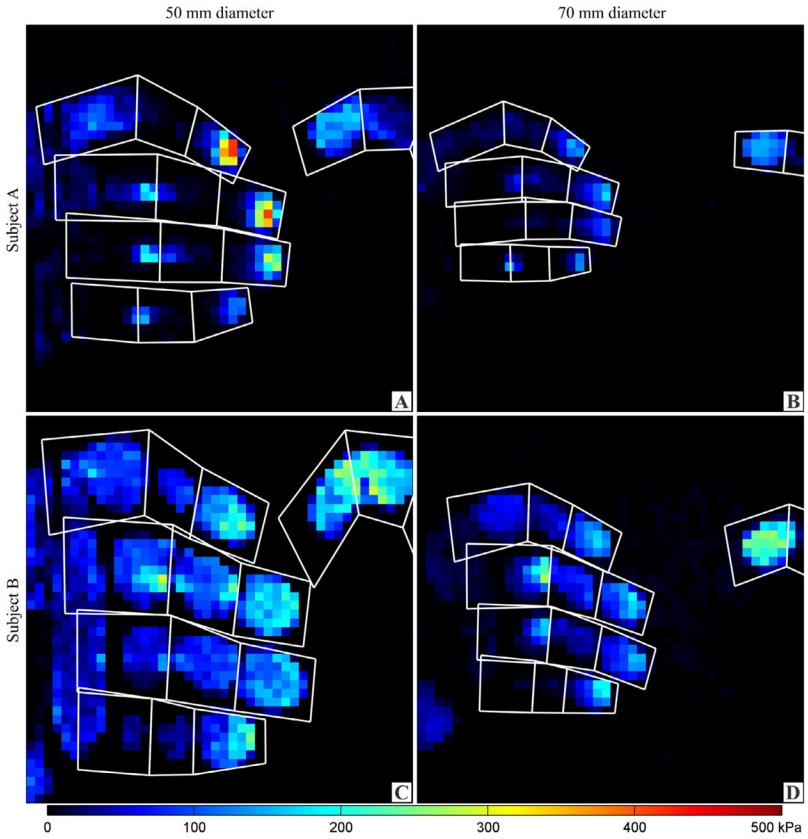

Fig. 5.

Grip pressure maps with phalangeal regions of interest for a combination of subjects and handle sizes. Each panel (A–D) contains a single pressure sample of a maximum voluntary grip trial. Each row is a single subject; anthropometry is given in Table 1. The left and right columns show results from the 50 mm and 70 mm handle, respectively. Each panel represents a 44 × 44 grid of pressure cells, where cells in the left and right columns have 2.54 mm and 3.75 mm side length, respectively. All panels share a uniform pressure scale in kilopascals, at bottom.

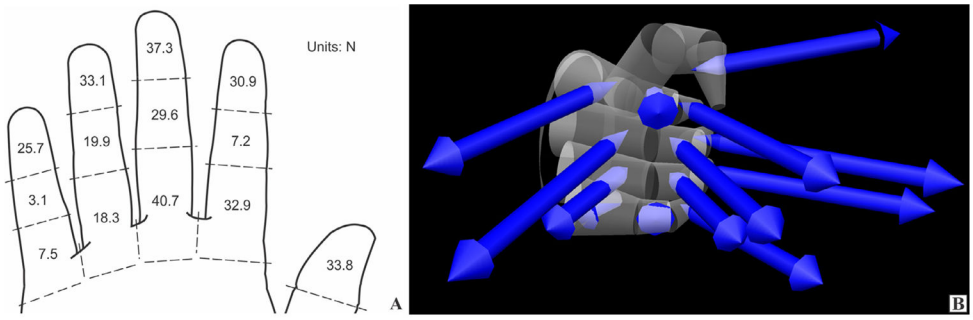

Fig. 6.

Phalangeal contact forces for Subject B with the 50 mm handle. (A) Force magnitudes for illustrated finger segments. (B) Cylinder reaction force vectors combined with the kinematic hand model in Visual3D software, using the corresponding COP locations in laboratory coordinates. The results were calculated from the sample reported in Fig. 5C. Forces were not calculated for the middle and metacarpal phalanges of the thumb, as those ROIs were not entirely within the pressure film.

Table 1

Human subject details. Hand length was measured as the distance from the distal wrist crease to the tip of the long finger with the hand extended [30]. Measurements are centimeters and kilograms.

Subject	Gender	Age	Stature	Hand length	Body mass
A	F	21	158	16.5	56.5
B	M	39	191	20.6	117.7

Table 2

Pressure film kinematic calibration errors. For the subject trials, RMSE is of 8 to 10 markers per frame with the mean (SD) calculated across 100 frames. Errors are between marker and nominal cell centroid in the calibrated grid. For replicated calibrations with a handle 47 mm in diameter, the RMSE and error vector magnitude (||**e**||) is of 10 markers of a single frame. The pressure film was optically scanned in a flatbed scanner and imported into vector graphics software (CorelDRAW X6, Corel Corp., Ottawa Ontario, CA), where errors were manually measured between marker and cell centroids. The same experimenter performed all calibrations. Measurements are in millimeters.

Subject trial calibrations		
Subject	**Handle diameter**	**Mean RMSE**
A	50	0.41 (0.01)
A	70	0.35 (0.01)
B	50	0.49 (0.02)
B	70	0.32 (0.01)
Replicated calibrations		
	Mean ||**e**||	RMSE
Trial 1	0.14 (0.08)	0.39
Trial 2	0.12 (0.09)	0.41
Trial 3	0.14 (0.08)	0.37

Table 3

Phalanx surrogate validation results. The F-score (F_1), is the unweighted harmonic mean of precision and the true positive rate (*TPR*), and has range [0, 1], where higher is better.

Handle diameter	Precision	TPR	F_1
50 mm	0.942	0.973	0.957
70 mm	0.945	0.972	0.959